



Long-Term Rain Attenuation Measurement for Short-Range mmWave Fixed Link Using DSD and ITU-R Prediction Models

O. Zahid¹  and S. Salous¹ 

¹Department of Engineering, Durham University, Durham, UK

Special Section:

The 33rd General Assembly and Scientific Symposium (GASS) of the International Union of Radio Science (URSI)

Key Points:

- Rain attenuation prediction in the mmWave band using rain statistics and fixed links radio data
- Long-term study through measured and predicted rain attenuation
- Attenuation measurement as a function of rainfall intensity, raindrop distribution, dominant drops, and drops diameter

Correspondence to:

S. Salous,
sana.salous@durham.ac.uk

Citation:

Zahid, O., & Salous, S. (2022). Long-term rain attenuation measurement for short-range mmWave fixed link using DSD and ITU-R prediction models. *Radio Science*, 57, e2021RS007307. <https://doi.org/10.1029/2021RS007307>

Received 1 MAY 2021
Accepted 29 MAR 2022

Author Contributions:

Conceptualization: O. Zahid
Data curation: O. Zahid
Formal analysis: O. Zahid
Investigation: O. Zahid, S. Salous
Methodology: O. Zahid
Resources: O. Zahid, S. Salous
Software: O. Zahid
Supervision: S. Salous
Validation: O. Zahid, S. Salous
Visualization: O. Zahid
Writing – original draft: O. Zahid
Writing – review & editing: S. Salous

Abstract Several millimeter Wave (mmWave) bands, which suffer from rain attenuation, were identified in the World Radiocommunication Conference 2019 (WRC-19) for fifth generation (5G) radio networks. In this paper, long-term attenuation is measured over typical building to building radio links in the built environment, which constitute two 36 m links along a direct link and an indirect side link at 25.84 and 77.54 GHz and a 200 m link at 77.125 GHz. The attenuation was also estimated using precipitation data from a high end accurate disdrometer weather station using the drop size distribution and the International Telecommunication Union (ITU) models. The results indicate that attenuation using Mie theory is in agreement with the ITU model for most of the rainfall events; with higher attenuation being measured than predicted when snow grains and raindrops mix. Raindrops with diameter between 0.1 and 4 mm indicate that the dominant raindrops have considerable influence on the measured attenuation, especially at light and moderate rainfall events. The maximum distance factor restriction of 2.5 in ITU-R P.530-17 is shown not to be suitable for short-range fixed links as it excessively underestimates attenuation.

Plain Language Summary Next generation mobile radio networks, 5G, are assigned several frequencies in the millimeter wave band, which are likely to suffer from rain attenuation. This can lead to outage in the communication link. This paper presents results of measurements and prediction models in the millimeter wave band using weather statistical data and radio data.

1. Introduction

The World Radiocommunication Conference 2019 (ITU-WRC, 2019) identified several mmWave frequency bands (24.25–27.5, 37–43.5, 45.5–47, 47.2–48.2, and 66–71 GHz) for possible allocation for the International Mobile Telecommunications (IMT-2020) for 5G applications and 71–81 GHz for non-geostationary fixed-satellite services. These higher frequency bands are largely affected by rainfall. The wavelength in the millimeter wave band ranges from 11 mm at 26 GHz decreasing to 1 mm at 300 GHz (Hemaddeh et al., 2017), while the diameter of the raindrops is on the order of 1 ~ 10 mm. Since the water permittivity also differs from free space (complex value; Durgin, 2000) an electromagnetic wave incident on rain drops will suffer from scattering which causes attenuation in the received signal strength (Nazar Elfadil et al., 2005).

Rain attenuation studies need long-term measurements and analysis over several years (Chandra Kestwal et al., 2014; Lam et al., 2017) to provide telecommunication network providers with accurate and useful results to plan and optimize reliable 5G radio links during precipitation events. Two rain attenuation prediction models are generally used. These are the regression model, which uses rain rate and path attenuation statistics data for rain attenuation modeling in a specific region; and the physical model (Crane, 2003), which uses statistical information of rainfall and scattering caused by rain drops for providing accurate prediction that can be implemented in different regions. It is recognized that the physical models depend mainly on precipitation conditions. Due to the unpredictable behavior of rain distribution and weather conditions, this imposes significant challenges and therefore a universal drop size distribution (DSD) is not feasible as it differs between regions: tropical region, dry, polar, continental, and coastal region (Åsen & Gibbins, 2002). Most of the rain attenuation studies report measurements based on long-range line of sight fixed links. In Kvicera et al. (2011), a fixed link, which operates at 93 GHz over 850 m is reported where the predicted attenuation using the ITU-R model provides a lower estimate than the measurements for high attenuation levels. In Schleiss et al. (2013), a link was set up at 38 GHz over 1.85 km with the aim to study the rain attenuation and the wet antenna effect where 2.5 dB maximum wet antenna effect was found. Results in Luini et al. (2018) provide reliable rain attenuation values compared to the DSD at 73, 83, 148, and 156 GHz with a link distance of 325 m. Results in Kim et al. (2013) show a significant

© 2022. The Authors.

This is an open access article under the terms of the [Creative Commons Attribution License](https://creativecommons.org/licenses/by/4.0/), which permits use, distribution and reproduction in any medium, provided the original work is properly cited.

difference between the International Telecommunication Union (ITU) model and the measured attenuation with the conclusion that the ITU model is not suitable for rain intensity above 100 mm/hr at 73 and 83 GHz for 500 m links. In Juttula et al. (2019), the scattering effect and attenuation were reported at 100 and 500 m at 60 and 300 GHz where the difference between the DSD and the ITU model reaches 5 dB.

Several works have reported rain attenuation prediction using rain statistics only. In Åsen and Gibbins (2002), a DSD model is used to quantify rain attenuation at 57, 97, 135, and 210 GHz at Chilbolton and Singapore. Their results indicate that the DSD differs with climatic condition levels of pollution. At higher frequencies and high rainfall rate, inconsistency and fluctuations were observed between the ITU model and the DSD attenuation model, with lower attenuation values predicted by the ITU-R model. In Tuhina et al. (2018), rain attenuation measurements were conducted for 22 GHz, 23 GHz, and 31.4/30 GHz in a tropical region: Kolkata in India and Belem in Brazil for 2 years. Results show good agreement between the DSD attenuation model and the ITU-R model for rainfall rate below 100 mm/hr, with slight differences below 30 mm/hr. In Saurabh et al. (2010), assuming a log-normal distribution for the DSD, both the DSD model and the ITU-R model gave similar results for frequencies below 30 GHz with a maximum rainfall rate up to 30 mm/hr in a tropical region.

In this paper, precipitation data are collected and used in the prediction models to estimate the rain attenuation in parallel with an mmWave channel sounder, which operates at two frequencies 25.84 GHz (K band) and 77.54 GHz, over two 36 m links: a direct link and an indirect link. Another link with a commercial radio frequency (RF) head is set up for continuous wave (CW) transmission at 77.125 GHz (E band) for attenuation measurements. Measurements are conducted from October to December 2020, and January 2021 for all three links. Since the rainfall rate is insufficient for the prediction of attenuation in the higher frequency bands, more accurate precipitation data are needed which include: rainfall rate, rain drop diameter, DSD, rainfall velocity, particle speed, and water permittivity. Such data can be obtained using a high end disdrometer station as used in the present study. The results of the attenuation prediction and measurement can be applied for regions with similar weather conditions. The ITU-R P.530-17 maximum distance factor restriction of 2.5 for short-range links is also investigated in addition to analyzing the effect of scattering of rain droplets.

This paper is organized as follows: the weather measurement system is presented in Section 2 together with rain statistics and raindrop distribution for the measurement period, followed in Section 3 by a description of the fixed link measurement setup for measuring attenuation and the ITU and the DSD prediction models. In Section 4, measurement results using the short-range fixed link data sets and the PWS100 disdrometer precipitation data are presented and compared for discussion; followed by raindrops induced scattering analyses in Section 5. Conclusions and ongoing work are presented in Section 6.

2. Precipitation Measurements for Rain Attenuation Modeling

2.1. Weather Station

A PWS100 Weather Sensor station was installed on the roof of the library at Durham University to record precipitations data as shown in Figure 1a. It is a laser based sensor capable of determining precipitation and visibility parameters (Scientific, 2015). Due to its developed measurement technique, the PWS100 can determine each individual particle type from accurate size and velocity measurements. The technical specifications of the station are listed in Table 1. The PWS100 disdrometer covers a measurement area of 40 cm². The station is controlled remotely to store data through the campus wireless network and the CR1000 data acquisition as shown in the block diagram of the measurement system in Figure 1b over an internet protocol address once every minute.

Figure 2a illustrates the rainfall intensity statistics between October 2020 and January 2021, with most of the measured rain intensity being under 20 mm/hr. In the results section, the rainfall intensity in mm/h is mapped against the received signal in dBm to estimate the rain attenuation in (dB) over the measurement period. Five types of rainfall intensities are used to investigate rain attenuation: light rainfall ($R \leq 1$ mm/hr), Moderate (1 mm/hr $< R \leq 4$ mm/hr), heavy (4 mm/hr $< R \leq 16$ mm/hr), very heavy (16 mm/hr $< R \leq 50$ mm/hr), and torrential rainfall ($R > 50$ mm/hr).

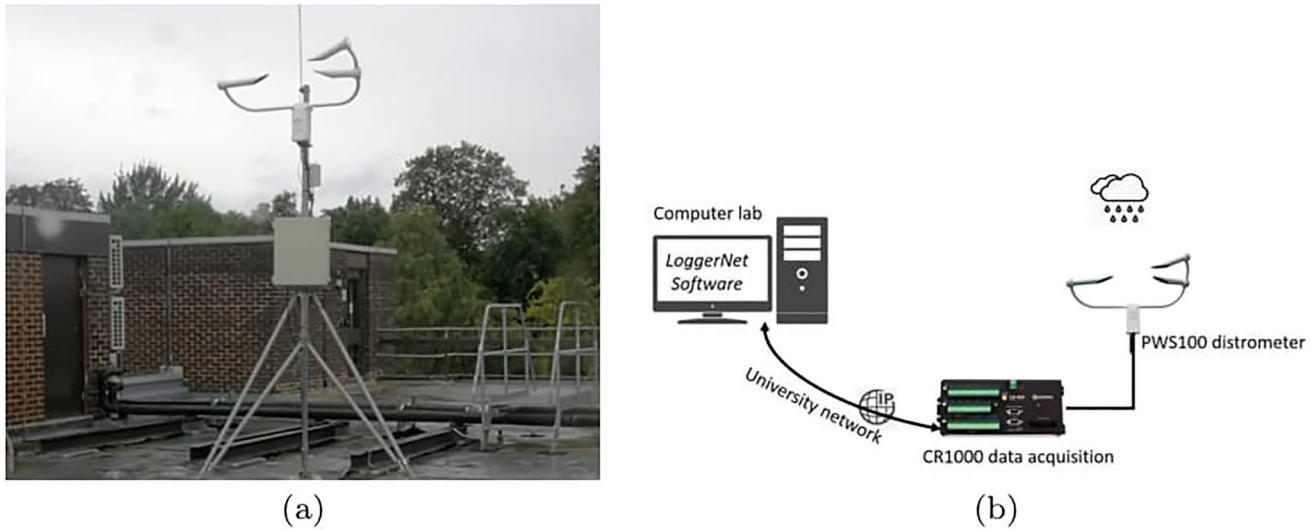


Figure 1. Weather measurement system installed on the roof of Durham University's library: (a) PWS100 weather station and (b) Block diagram.

2.2. Drop Size Distribution

Raindrop Size Distribution (DSD), noted by $N(D)$, plays a critical role in determining the microphysics of rain (Marshall & Palmer, 1948). It has a significant role in radio propagation performance links. The DSD varies and depends on the location. For a given rainfall type, we could get two different types of DSDs which result in different values of signal attenuation. Using the PWS100 disdrometer, the DSD is recorded with 300 values of the number of drops corresponding to the diameter from 0.1 to 30 mm with 0.1 mm resolution. The DSD can be calculated as:

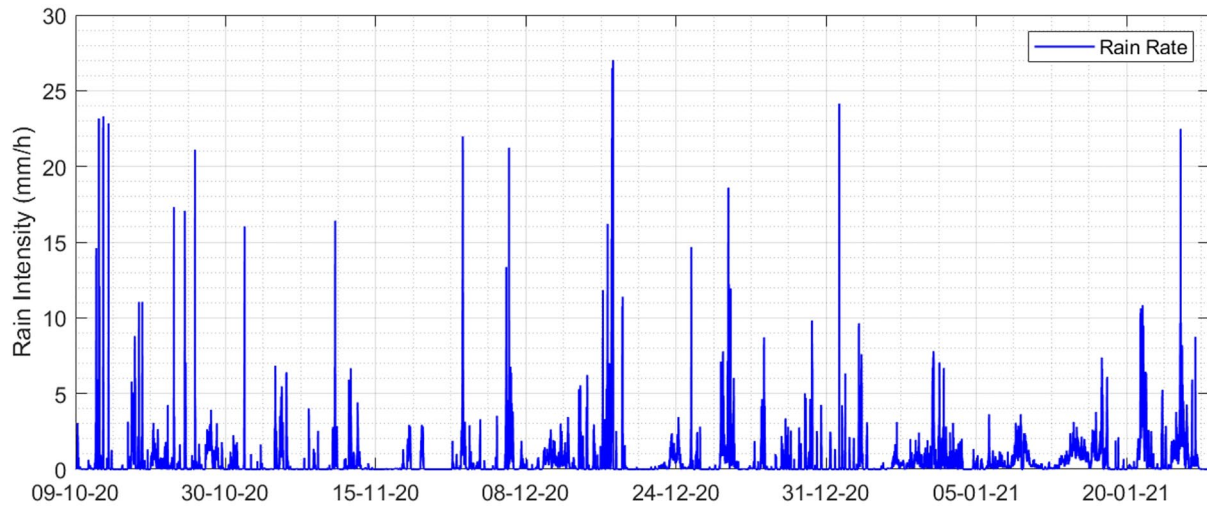
$$N(D_i) = \sum_{j=1}^{300} \frac{n(D_i, v_j)}{v_j} \cdot \frac{1}{S \cdot \Delta t \cdot dD_i} \quad (1)$$

where $S = 40 \text{ cm}^2$ is the measurement surface of the laser beam of the PWS100 disdrometer, $t = 60 \text{ s}$ is the integration time, $n(D_i, v_j)$ is the number of particles registered within the classes with mean diameter $D_i(\text{mm})$ and mean speed $v_j(\text{m/s})$, and $dD_i(\text{mm})$ is the class width associated with the diameter D_i . The PWS100 can determine each individual particle type from accurate size. For each minute, we have the corresponding rain rate and number of drops for each bin and the following steps take place for the average DSD:

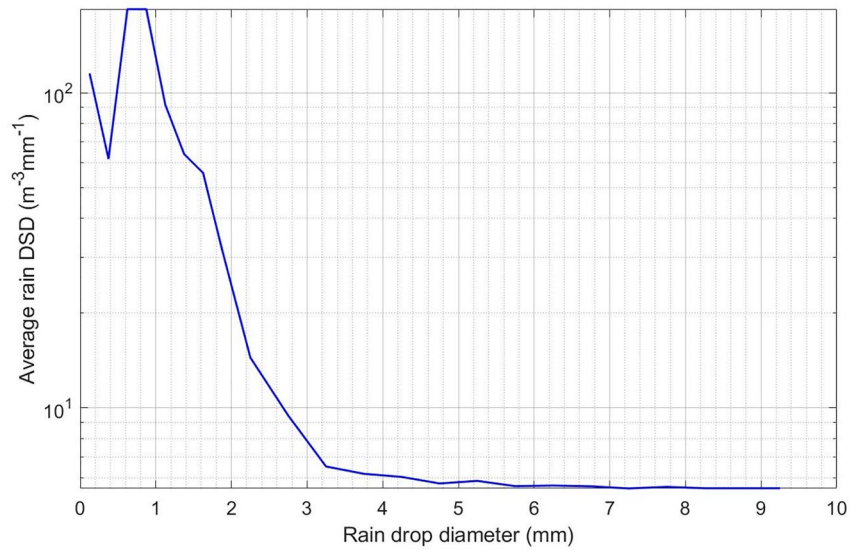
1. The integration time intervals of disdrometer measurements are to be categorized according to the desired rain rate classes, for example, 5 and 20 mm/hr.
2. For each long-term mean (i.e., in each rain rate class) the disdrometer bin size classes are to be rearranged according to the bin size classes (0.1, 0.2, and 30 mm).

Table 1
Specifications of the PWS100 Weather Station

Parameters	Specifications
Particle diameter	0.1–30 mm
Size accuracy	5% (for particles >0.3 mm)
Particle velocity	0.16–30 m/s
Velocity accuracy	5% (for particles >0.3 mm)
Types of precipitation	Drizzle, rain, snow grains, snowflakes, hail, ice pellets, graupel, and mixed
Rain rate intensity range	0–400 mm/hr
Rain total accuracy	Typically 10%



(a)



(b)

Figure 2. Precipitation measurement: (a) Continuous rain rate measurements between October 2020 and January 2021 in Durham, England and (b) the measured drop size distribution from the PWS100 disdrometer.

3. The (long-term mean) drop count in each bin size class is to be divided by the measuring area (of the instrument 40 cm^2) and by the column height (integration time multiplied by the mean fall velocity of this bin's mean diameter). Thus the (long-term mean) drop counts per unit volume are obtained.
4. To obtain the required distribution density further in each bin size class the drop counts per unit volume are to be divided by the bin size class width.

Appropriate unit conversions are implemented to deliver the result in $(\text{m}^{-3}\text{mm}^{-1})$. Figure 2b reports the measured DSD where the peak DSD occurs at around a raindrop diameter of 0.8–1.2 mm for most of the rain events.

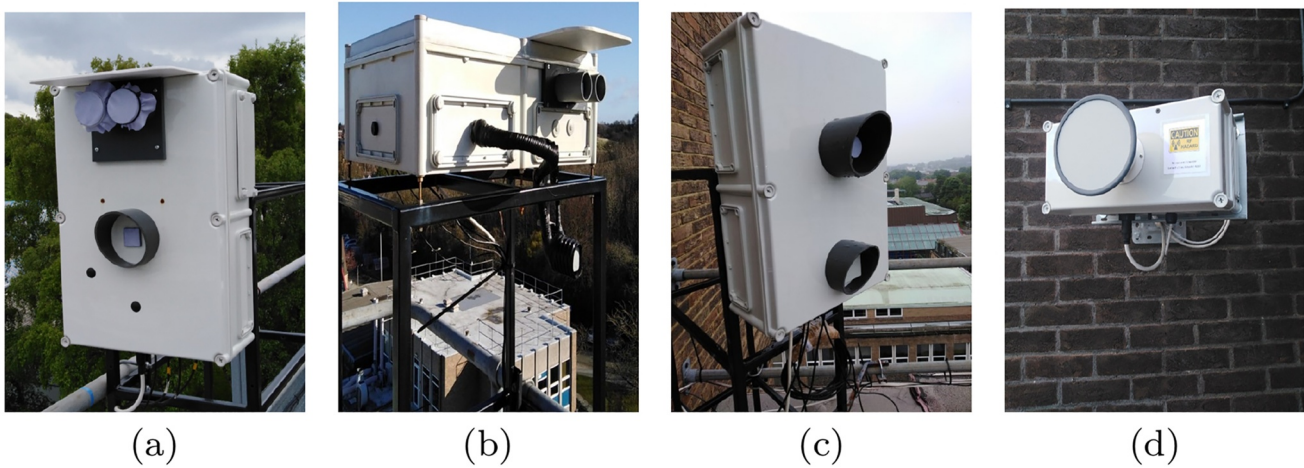


Figure 3. Fixed link radio frequency heads of the measurement setup, (a) transmitter box for 36 m link, (b) receiver box for direct 36 m link, (c) receiver box for side 36 m link, (d) transceiver Filtronic box for 200 m link.

3. Prediction of Rain Attenuation

3.1. mmWave Fixed Link Channel Sounder Setup

The experimental fixed link setup described in Salous et al. (2019), Huang et al. (2019), and Zahid et al. (2020) used for collecting fixed link data for real rain attenuation investigation is shown in Figure 3. The first two links are set up over a direct path and side path over 36 m links and located on the rooftop of the Engineering department at Durham University (Latitude: 54.767396, Longitude: -1.570390) at 65 m of sea level elevation. Two antennas with vertical and horizontal polarizations are used for the E band and a dual polarized antenna is used for the K band for the direct link. To study the effect of scattering and interference a second side link receiver was installed. For the side link Rx, single vertically polarized antennas were used for both the K band and the E band. Custom designed covers were installed for all the antennas to reduce the impact of the wet antenna effect on the measured attenuation. The fixed link operates on CW transmission (building to building/lamppost to lamppost scenario). The third link which operates at 77.125 GHz is installed between Durham University Library roof (Latitude: 54.768167, Longitude: -1.573418) at 62 m of sea level and the engineering department roof which gives a point to point 200 m path. The Tx/Rx for the 200 m link are commercial transceivers (Filtronic Orpheus E-band modules) shown in Figure 3d. The transceiver groups the Orpheus interface board, a NI USB-8451, and an electronic circuit power to supply the module. Once mated, the module can be powered up using standard lab PSUs (-5 V, $+2.8$ V $+3.3$ V, and $+5.1$ V $+18$ V). For the control of the module, a NI USB-8451 is used with the Filtronic Orpheus GUI software. The 200 m point-to-point link is named figuratively “Filtronic link.” The three links are remotely controlled through the campus internet network and data are recorded for each minute, simultaneously with the weather station data. The channel data are recorded for 1 s every minute to relate with the rain rate data. The sampling rate of the RF link is 80 MHz and the attenuation per minute is an average of 1 s, as the baseband signal frequency is at 4, 12, and 31 MHz, respectively.

3.2. Prediction Models

Rain attenuation affects the Quality of Service of radio links in the millimeter wave bands. It is therefore vital to have accurate and reliable propagation models for predicting rain attenuation using precipitation data such as rainfall rate, DSD, velocity, temperature, and water permittivity. The prediction models used in this study are the ITU-R P.838-3 model and the DSD model, which use frequency parameters, wavelength, water permittivity, and raindrop distributions (Shrestha & Choi, 2017).

3.2.1. ITU-R P.838-3 Model

This model was validated theoretically and experimentally and is recommended for the frequency range from 1 to 1,000 GHz. It is given by:

Table 2
k and α Coefficients

	26 GHz	77 GHz
<i>k</i> (vertical)	0.1669	1.1276
<i>k</i> (horizontal)	0.1724	1.132
α (vertical)	0.9421	0.7073
α (horizontal)	0.9884	0.7177

$$\gamma = kR^\alpha \quad (2)$$

where R is the rainfall rate (mm/h), k and α are model parameters, which depend on the frequency f (GHz), and γ is the specific attenuation in dB/km. The ITU recommendation provides a look-up table of the values k and α for different frequencies for both the vertical and horizontal polarization (Recommendation ITU-R P.838-3, 2005) are noted in Table 2.

The total attenuation for a specific distance depends on the effective path length d_{eff} between the Tx and Rx antennas as:

$$A = \gamma d_{eff} \quad (3)$$

where the effective path length, d_{eff} of the link is obtained by multiplying the actual path length d by a distance factor r , from ITU-R P.530-17 as

$$r = \frac{1}{0.477d^{0.633} R_{0.01}^{0.073\alpha} f^{0.123} - 10.579(1 - \exp(-0.024d))} \quad (4)$$

where $R_{0.01}$ is the rain rate exceeded for 0.01% of the time (with an integration time of 1 min). In ITU-R P.530-17 it was recommended to use a maximum value of r equal to 2.5 while in the updated recommendation P.530-18, the restriction on the maximum value of r has been removed. For the present study, results with and without the restriction of $r = 2.5$ are compared with the measured attenuation for our short-range fixed links for both frequency bands.

3.2.2. Drop Size Distribution Model

The attenuation using the DSD model based on Mie theory in Bohren and Huffman (1998) is given as:

$$\gamma = 4.343 \times 10^3 \int_0^\infty \delta_{ext}(D)N(D)dD \quad (5)$$

where γ is the specific attenuation in dB/km, $\delta_{ext} = \pi \left(\frac{D}{2}\right)^2 Q_{ext}$ is the extinction cross section (m²) for water drops of diameter D (mm), and $N(D)$ is the measured DSD value (m⁻³ mm⁻¹) at diameter D from the sensor weather station PWS100. The extinction efficiency Q_{ext} can be calculated from Mie scattering or Rayleigh scattering theory depending on the size parameter $X = \pi D/\lambda$, where λ is the wavelength.

For the current rain attenuation prediction, we use the measured DSD from the PSW100 weather station. The disdrometer records only fall velocity and not for each particle; hence, we use Equation 6 given in Atlas and Ulbrich (1977) and Atlas et al. (1973) for the calculation of particle speed. The DSD can also be calculated using theoretical and analytical models such as: the Marshall-Palmer (M-P) distribution (Marshall & Palmer, 1948) and the Weibull distribution (Jürg & Enrico, 1978). In this study, we use the measured raindrop distribution from the PWS100 disdrometer. For comparison, we consider the widely used Gamma distribution, given by Ulbrich (Carlton, 1983) in Equation 7.

$$v(D_i) = \{3.78D_i^{0.67}, D_i < 0.8 \quad 9.65 - 10.3e^{-0.6D_i}, D_i \geq 0.8\}. \quad (6)$$

$$N(D) = N_0 D^\mu \exp(-\lambda D) \quad (0 \leq D \leq Dmax) \quad (7)$$

where D (mm) is the rain drop diameter, N_0 is the intercept parameter, μ is the shape parameter, and λ is the slope parameter, and the mean value of μ is 3 (Kumar et al., 2010; Nabangala, 2016). Gamma distribution given in Ulbrich model is applied to fit the rain DSD and used for comparison purpose only. The theoretical relation between the terminal fall velocity and the drop dimension is taken for the DSD calculation because the velocity of each particle is not measured.

$$N_0 = 1.41 \times 10^6 R^{-0.52} \quad (8)$$

$$\lambda = 9.48 \times R^{-0.2} \quad (9)$$

Table 3
The Complex Refractive Index of Water

Frequency	Water refractive index
26 GHz	5.41 + 2.78i
77 GHz	3.64 + 1.84i

The type of scattering effect depends on the extinction efficiency which relies on m the complex refractive index of water; which is related to temperature and frequency (Schiebener & Straub, 1990). Throughout the measurement period, an average computation was used on the temperature. The average temperature was 7° and the complex refractive index of water was calculated according to Table 3 for each frequency band. Figure 4 presents the extinction efficiency as a function of size parameter X , where Mie theory calculations have been implemented to calculate the extinction efficiency. It should be noted that X refers to Mie size parameter as a function of diameter

D , λ , and π . When the rain drop is much smaller than the wavelength $X \ll 1$, $D < \lambda$, the probability of scattering increases and the wavelength decreases, that is, Rayleigh scattering. Mie scattering takes place when $X \approx 1$, while geometric optics scattering occurs when $X \gg 1$.

The high capability measurement of the disdrometer provides for each minute the corresponding rain intensity, number of recorded droplets for each diameter type, the temperature, the fall velocity, and humidity. For each rainfall, the dominant number of drops is extracted. Figure 5 displays the parameters that have significant impact on the attenuation behavior computed from the collected precipitation data throughout the measurement period. At each raindrop diameter, the figure displays the maximum number of drops found from the total rain statistics, its speed in m/s, and the corresponding rain intensity. An exponential variation of particle speed up to 5 mm drop size is observed, beyond which the velocity flattens out. The number of drops is seen to be in the range of 25–250, while most of the raindrops size falls between 0.1 and 2 mm.

Because previous data sets in the paper we published in Huang et al. (2019) revealed a significant wet antenna effect, the present study provides results following extensive updating of the measurement link setup along with longer term measurement campaign than before, which reduces the antenna wetness effect by placing antenna hoods and integrating the IF unit with the RF heads. In addition, long-term measurement disdrometer meteorological data from the PWS100 of 3 years are now available. The data are being submitted and used for the ITU-R Study Group 3 data sets bank.

4. Discussion of Measurement Results

This section presents the calculated attenuation at 25.84 GHz (K band) and 77.54 GHz (E band) over the two 36 m links between October 2020 and January 2021 and the 77.125 GHz band over the 200 m link from November 2020 to January 2021 adopting the ITU and DSD models for comparison with the measured rain attenuation

for which the data availability ratio for direct and side 36 m links is 82.55% and 70.47% for the 200 m link. Vertical to vertical polarization, which is common to all the three links is selected for the two bands over 252 hr of rain data. The attenuation is calculated and referenced using sunny clear sky days before and after the recorded data. We perform the following steps to measure the attenuation: initially, a reference signal is obtained for sunny and clear sky hours chosen before the rainfall event; then subtract from the reference signal the received signal during the rain event. The data are verified each minute to ensure reliability and to avoid loss in the signal due to the measurement system rather than rain. Measurement days where snow occurs are compared to rainy days. The attenuation is mapped against the rain intensity. The effects of raindrop diameter distribution, and diameter of the dominant drops on the measured attenuation are presented. The measurements through this period include some gaps of no rain hours and days while 218 hr of light rainfall data, 32 hr of moderate rainfall data, 3.4 hr of heavy rainfall data, and around 25 min of very heavy rainfall data were recorded. Predominant and frequent rain events were identified for calculation and modeling of the rain attenuation. For accurate and reliable rain attenuation study, minutes corresponding to equipment transient behavior (rising and drop of the received power), the power flatness of the system, atmospheric attenuation, equipment

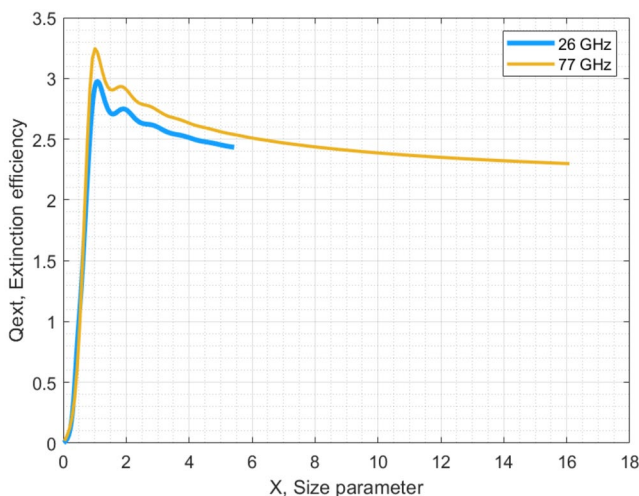


Figure 4. Extinction efficiency versus size parameter X for the selected frequency bands.

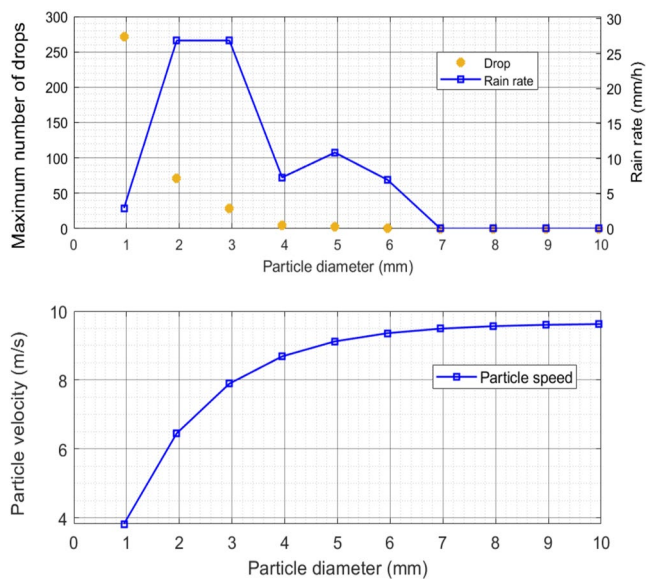


Figure 5. Particle velocity variation versus its diameter and the number of maximum drops for each particle type for the measurement period of October 2020–January 2021.

icing, humidity, and wind are not used in the analysis. For each link, the best measured data sets and the most stable signal strength are used for the estimation of the attenuation.

4.1. Predicted Attenuation

The estimated rain attenuation using the disdrometer data is presented for both the ITU and DSD model. The rain attenuation is classified into two categories: (a) physical, which uses the measured radio link data for rain loss calculation to integrate it into the radio channel parameters for link budget calculation and (b) modeled attenuation, which predicts the attenuation using the DSD model based on Mie scattering theory given by Equation 5 using the disdrometer data and the ITU-R prediction model given in Equation 2. When measuring and calculating rain attenuation with rain intensity statistics, raindrop distributions, and particle size, various parameters such as atmospheric conditions (Han & Duan, 2019), scattering and interaction between raindrops, and absorption (Mora Navarro & Costa, 2016; Surco Espejo & Costa, 2017) need to be considered. In this study, it is assumed that the raindrops are spherical for Mie theory and scattering. The interactions between raindrops are negligible. Other climatic conditions such as wind, snow grains, snowflakes, and ice pellets are also not considered for rain attenuation through snow events but will be presented to show their effect on the signal strength. As shown in Figure 4, the size parameter X is 5 and 16 for 26 GHz, and 77 GHz, respectively. At higher frequency, the extinction efficiency approaches 2.5 and the size parameter is greater than 10 (larger raindrops) almost near to geometric cross section area, when Mie theory is applied.

Equations 5 and 2 are given for the specific calculation in dB/km, so the distance factor r should be taken into consideration when converting to the specific path lengths of 36 and 200 m. This factor was mainly derived from long-range measurements. Using the ITU recommended maximum value of 2.5 raises the question regarding its application for short-range links less than 1 km (Budalal et al., 2020; Huang et al., 2019; Olsen et al., 1978). Hence, the suitability of the maximum r factor is further investigated for the current short-range links.

Equations 5 and 2 are given for the specific calculation in dB/km, so the distance factor r should be taken into consideration when converting to the specific path lengths of 36 and 200 m. This factor was mainly derived from long-range measurements. Using the ITU recommended maximum value of 2.5 raises the question regarding its application for short-range links less than 1 km (Budalal et al., 2020; Huang et al., 2019; Olsen et al., 1978). Hence, the suitability of the maximum r factor is further investigated for the current short-range links.

Figures 6 and 7 show the calculated attenuation for the K and E bands using the ITU and DSD models for the 36 and 200 m, respectively. The figures indicate good agreement for most of the rain events, whereas during the snow events comparison with the DSD and the ITU is mainly derived from rain drops not snow grain and snowflakes; therefore, the DSD model shows higher attenuation values up to 4 dB than the ITU model since during the snow events the raindrop distribution is formed of a mixture of raindrops and snow particles. Consecutive heavy rainfall events show slightly higher attenuation using the ITU model at the E band for both links with 1.2 and 4 dB recorded for maximum rainfall rate of 5 mm/hr and 20 mm/hr, respectively, for the direct E band link while a maximum of 6 dB loss for 20 mm/hr for the 200 m link.

4.2. Measured Attenuation

The results of the measured attenuation as a function of rainfall up to 25 mm/hr are presented. Figures 8, 10, and 11 show the received signal mapped against the rain intensity and snow particles for the three links: direct 36 m, 200 m, and side 36 m, respectively, for the K and E band vertical to vertical polarization. The figures show that the signal strength follows the rainfall trend. During snow events, the signal takes more time to recover to the level following the end of rain/snow event due to antenna icing as can be seen in Figure 9. This effect should be differentiated from the measurement by eliminating from the analysis the icing events. Compared to the predicted-calculated attenuation as shown in Figure 12 (samples of dominant rainfall events through the measurement period and matched attenuation) the measured attenuation for the direct 36 m link during rain events without snow and before mid of December 2020 shows an average of 0.8–1.5 dB higher attenuation for heavy and very heavy rainfall at 26 GHz, while a difference of 0.4–1.3 dB at 77 GHz. However, higher losses up to 9.5 dB are recorded when a mixture between rain and snow occurs. The side link shows somewhat higher attenuation than

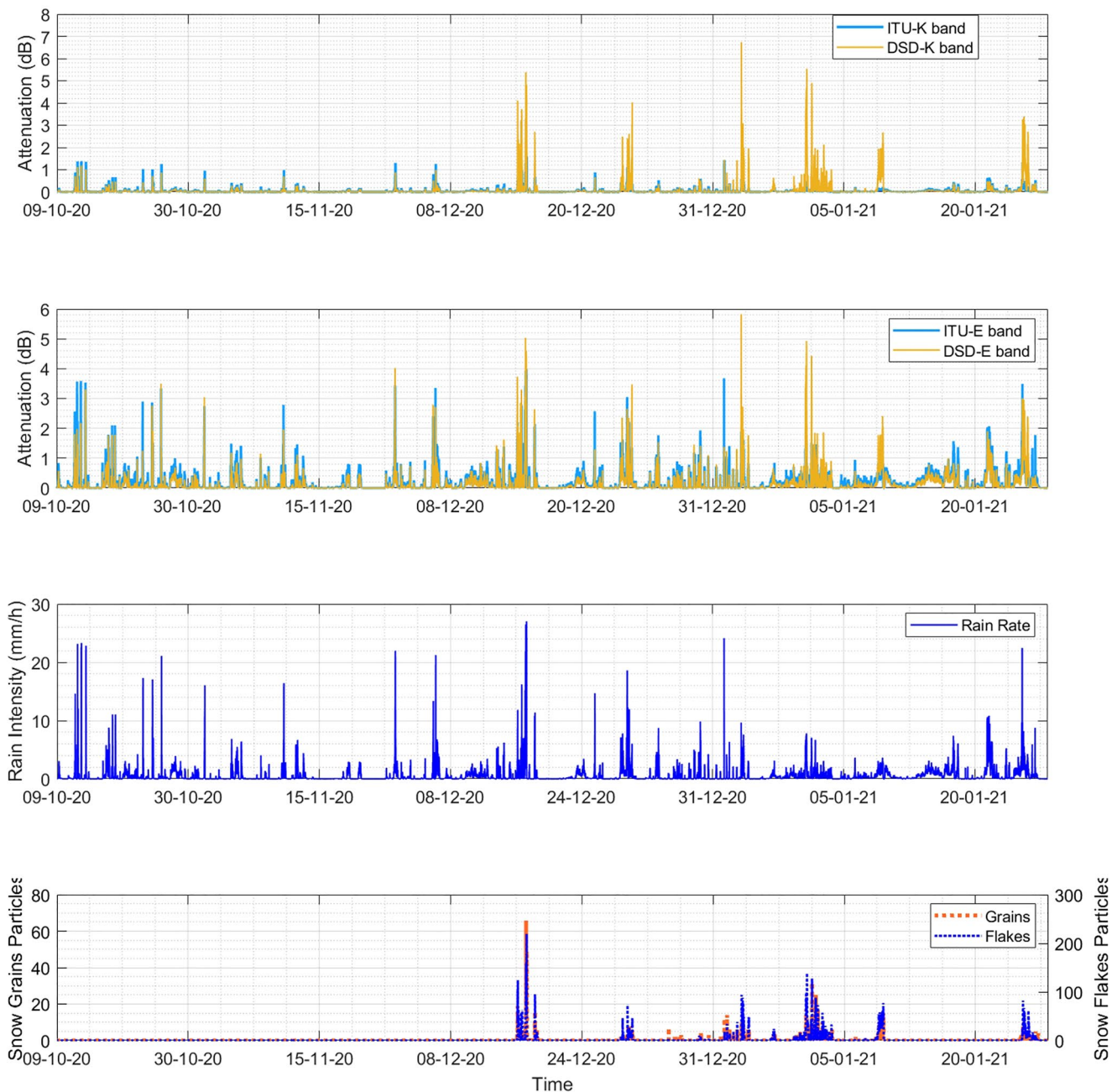


Figure 6. Predicted rain attenuation for K and E band over dominant recorded rainy days between October 2020 and January 2021 for 36 m link.

the direct link 0.5–2.3 dB as the side link depends on non-Line-of-Sight (NLOS) reflected paths to receive the signal. Thus, the measured attenuation is affected by raindrops scattering mechanism. The K band side link exhibits 1.7 dB difference with respect to the predicted rain attenuation for light, moderate, and heavy rainfall events. Measured rain attenuation for the 77 GHz 200 m link agrees well and follows the predicted attenuation for most rainfall events where 6 dB loss has been recorded for a maximum rain intensity of 20 mm/hr.

It can also be observed that the measured attenuation values are not all uniform with the rain fall rate and the calculated attenuation using the ITU and the DSD models using the disdrometer data. For instance, two similar rain intensities may result in two different rain attenuation values. As an example 11 mm/hr was recorded on 13 October 2020 at 10:17 and the 31 October 2020 at 12:58 result in 1.56 and 2.28 dB at 77 GHz, respectively. This is also observed in other works (Aydin & Daisley, 2002; Brazda & Fiser, 2015; Sander, 1975; Schönhuber

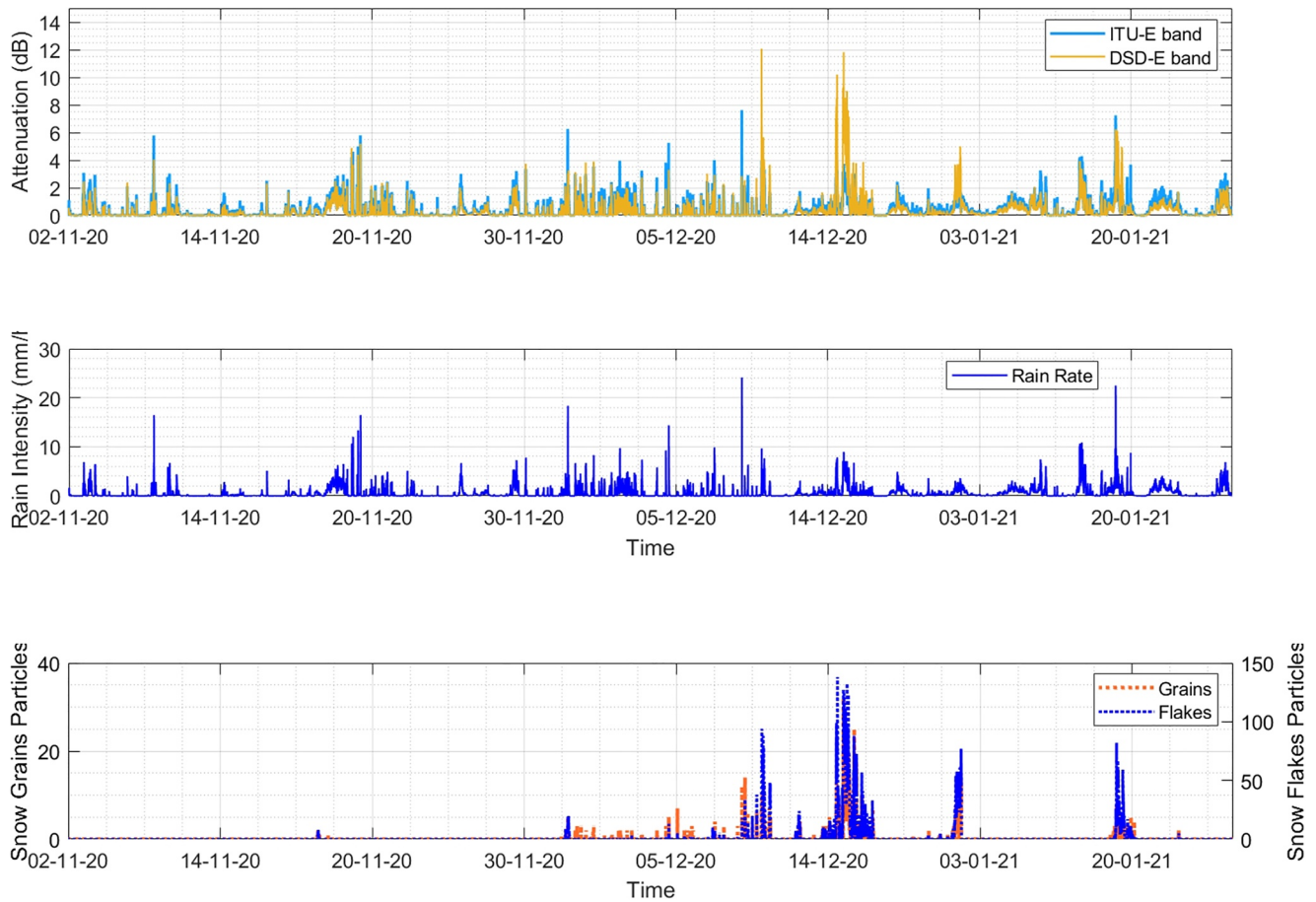


Figure 7. Predicted rain attenuation for E band over dominant recorded rainy days between November 2020 and January 2021 for 200 m link.

et al., 2015; Townsend et al., 2009). This instantaneous difference between the measured and the DSD/ITU calculated attenuation values could be due to a number of factors:

1. Mie theory assumes that rain drops are spherical, whereas it is not always the case within a real rainfall event since the DSD model uses real disdrometer data, which is subject to severe weather conditions that reduces its collection capability.
2. For light rain rate, the disdrometer might not be able to count small raindrops in higher windy situations.
3. Other factors that may affect the collected radio data are the humidity (Tamošinait et al., 2011) where the humidity continues its existence in the atmosphere in sunny clear days and temperature variability in space and time (Setijadi et al., 2009). In the DSD model estimation, the average monthly value of temperature was used and the humidity was neglected.
4. Successive rain events up to 10 hr (moderate rainfall events). The signal takes more time to recover after this long-term rain event.
5. The former method inherently assuming a constant analytical DSD for the derivation of the k and alpha coefficients in Equation 2.

The raindrops size and rain event distributions are not uniform within space and time due to the variability of raindrop distribution and the particle size, which corresponds to the number of each dominant raindrop diameter, rainfall speed, and particle speed. Mostly, for all rainfall types, raindrops size between 0.1 and 3 mm contribute to the maximum attenuation which is $\lambda/2$ at 77 GHz as shown in Figure 16. This indicates that the number of dominant raindrops has a significant influence on the specific attenuation, which can result with up to 2 dB difference at the same rainfall type within two different dates at the range of 0.1–2 mm drop size.

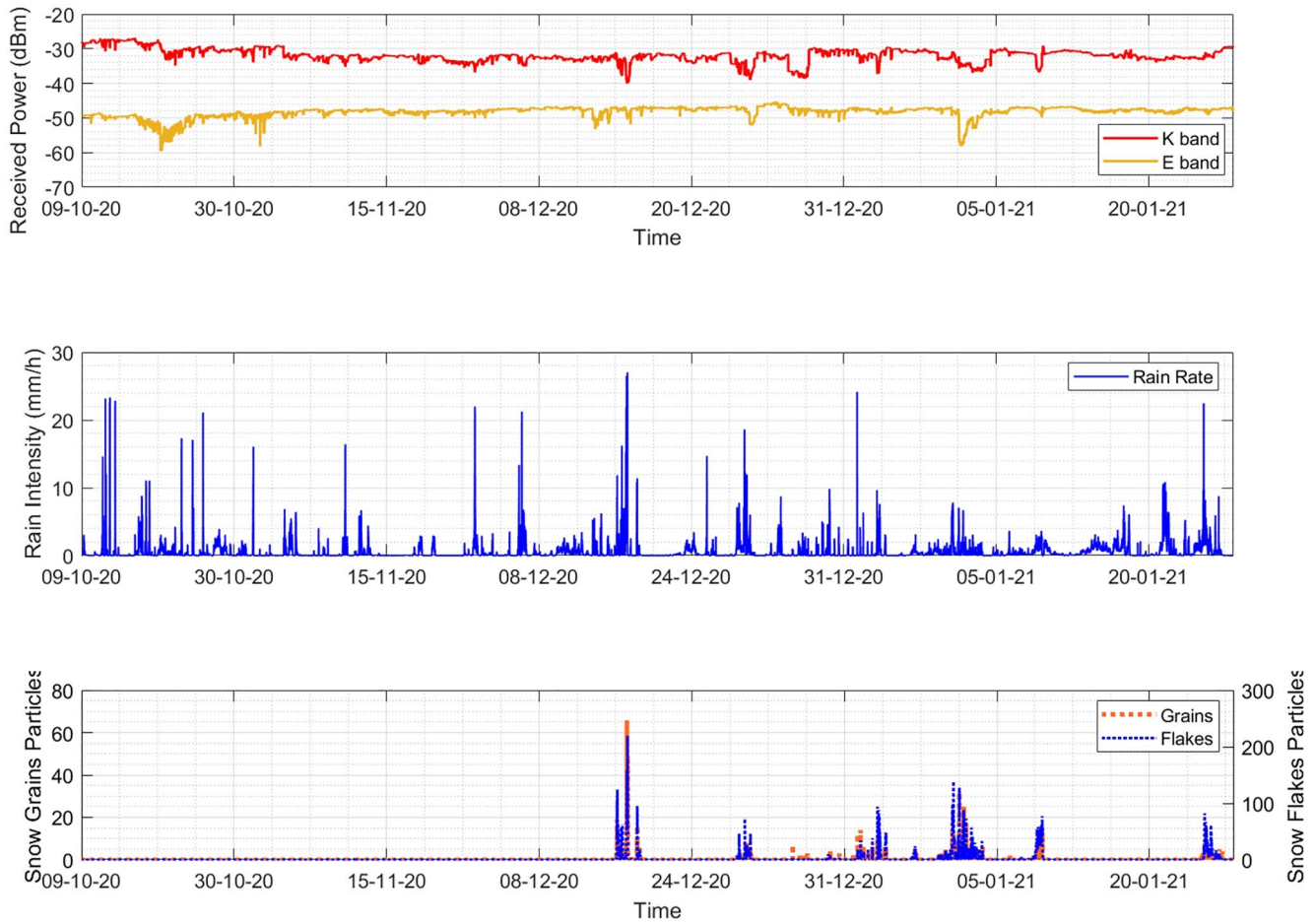


Figure 8. Long-term rain attenuation measurement for direct 36 m link at K and E band through dominant recorded rainy days between October 2020 and January 2021.

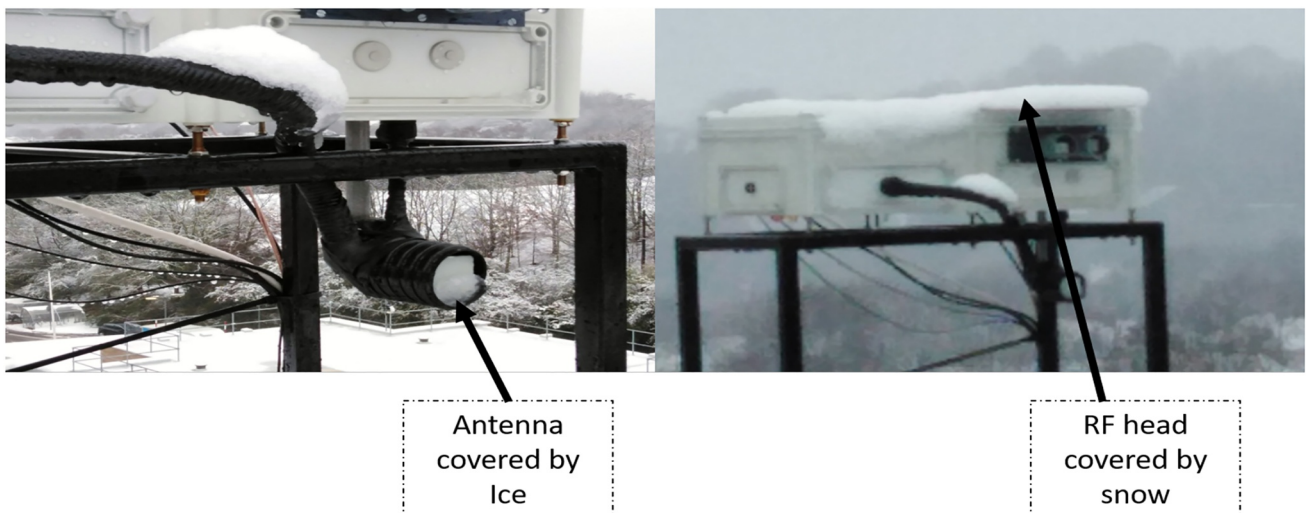


Figure 9. Effect of snow and ice on hardware measurement.

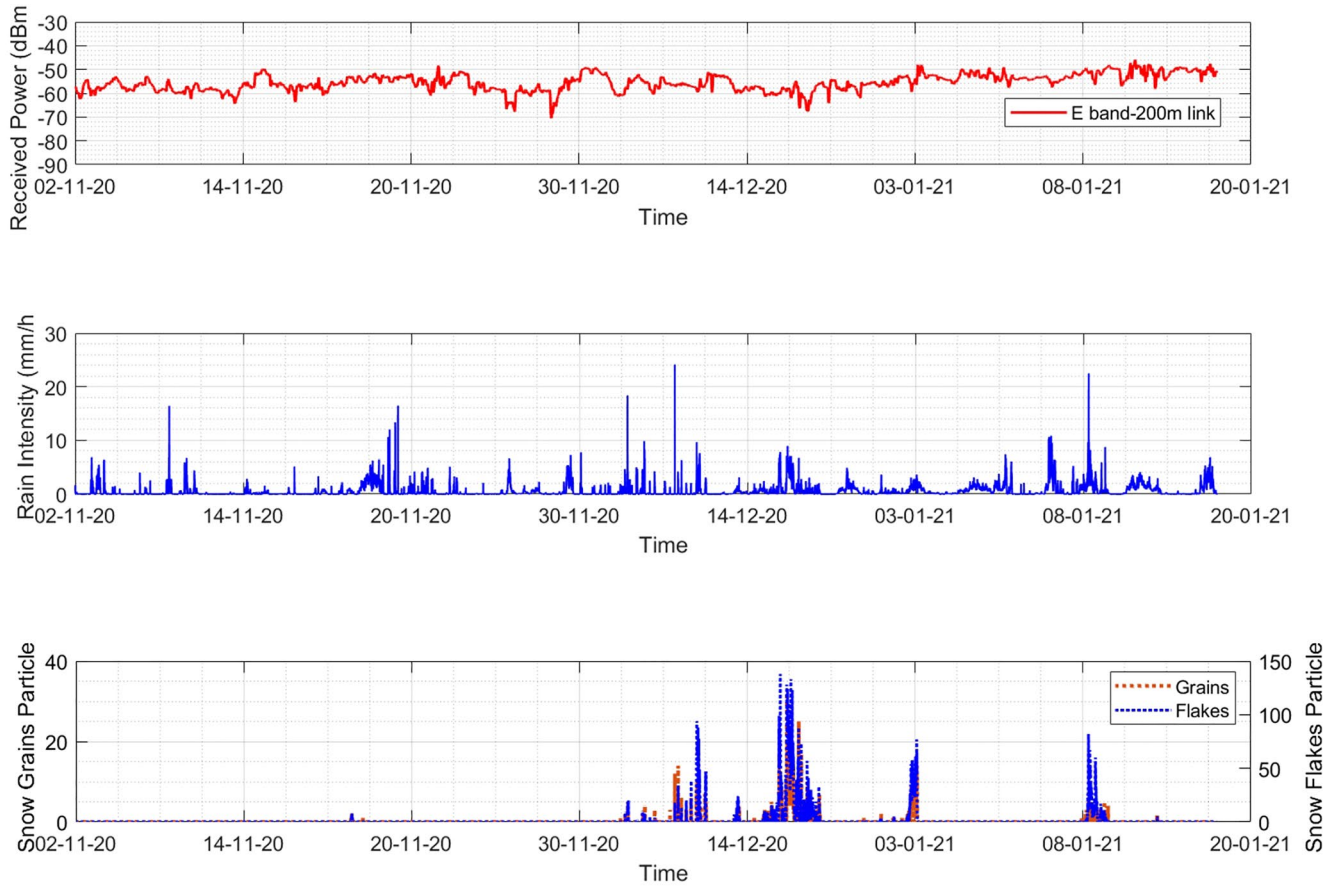


Figure 10. Long-term rain attenuation measurement for point to point 200 m link at E band through dominant recorded rainy days between November 2020 and January 2021.

In Figure 13 the measured CDFs are compared with the predicted CDFs from the ITU and DSD models. Good agreement between measured and calculated attenuation is obtained at 77 GHz for the direct, side, and Filtronic links. A notable difference occurs at the lower frequency band at 26 GHz between the measured and the theoretical values for the side link where the measured attenuation has larger values.

In addition, mmWave short-range fixed links require accuracy and reliability of prediction. The ITU-R P.530-17 model uses the effective path length for estimating the rain fade and r distance factor which is derived from long range measurements. It is recommended in the model to use a maximum value of $r = 2.5$ whereas in the updated recommendation, this restriction has been removed. The recommended value of r with and without the restricted value are implemented into the calculation, and thereafter investigated for the three links within its corresponding frequency bands. Figures 14 and 15 show a full and detailed comparison between the measured and ITU predicted rain attenuation using the maximum recommended distance factor and without using it for the E and K bands, respectively, where rain rate and attenuation were measured for each event in an instantaneous manner within 1 min interval. The results indicate that when the r value is restricted to 2.5, the predicted rain attenuation exhibits higher differences with the measurements than when it is not used at both frequency bands for both the 36 m and the 200 m links.

To further examine the impact of other rain parameters on the link, Figure 16 presents samples of measured attenuation versus raindrop diameter from 0.1 to 7 mm which were within different rainfall rates. The calculated attenuation using Mie theory is correlated to the relevant amount and type of droplets collected at that minute, thanks to the disdrometer's recording capabilities. The attenuation rises with the raindrop diameter. The highest attenuation is illustrated for the events where raindrops' diameters range between 2 and 4 mm. The analyzed results indicate that very heavy and moderate rainfall rate lead to higher attenuation values for both frequencies

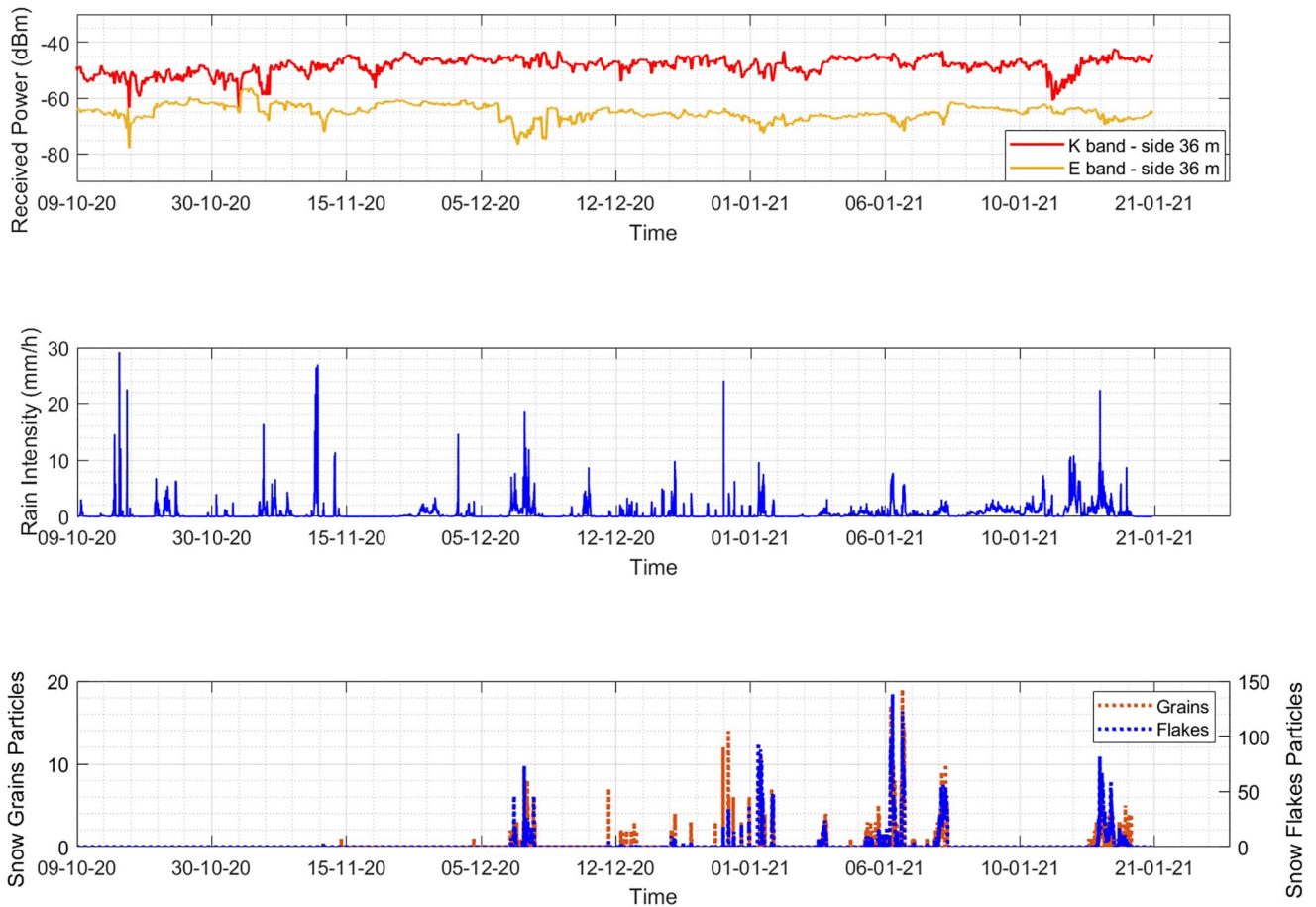


Figure 11. Long-term rain attenuation measurement for side 36 m link at K and E band through dominant recorded rainy days between October 2020 and January 2021.

in the presence of large rain drops (above 2 mm). Similar to the analyses in Figure 6 in the previous section and Figure 16, when the particle speed is 9–10 m/s even with a number of particles lower than 20 drops, it results in higher and variable attenuation specially for very heavy rainfall higher than 20 mm/hr where raindrops with the size of 1–3 mm lead up to 4.5 dB higher attenuation. A diameter in the range of 4–7 mm contributes occasionally to the attenuation up to 2 dB for both frequency bands. It should be highlighted that the computed rain attenuation value is matched for each rain rate event thanks to the weather station data measurement features, which include the associated temperature, drop distribution per diameter for each minute, and humidity provided. We can match the rain event to the matching raindrop size, which means that for example, if the event is 5 mm/hr, we can extract the number of drops for each drop size type and then select the dominant drop. This study found that higher rainfall and a greater number of rain droplets of predominant diameter lead to higher attenuation than the theoretical prediction with low rainfall.

Based on the computations, we identify the drop diameter region that contributes the most to overall attenuation. The phrase (maximum attenuation) refers to the maximum value that is obtained with that number of drops.

The next section elaborates raindrops scattering mechanism using the recorded disdrometer data and Mie theory.

5. Raindrops Induced Scattering

Scattering due to raindrops has a significant effect because rain scattering is considered one of the main sources of attenuation and interference (Olsen et al., 1993). Scattering can be governed as a function of wavelength (λ) of the incident radiation, the size of the scattering particle, usually expressed as the nondimensional size parameter, X , and the particle optical properties relative to the surrounding medium: the complex refractive index which

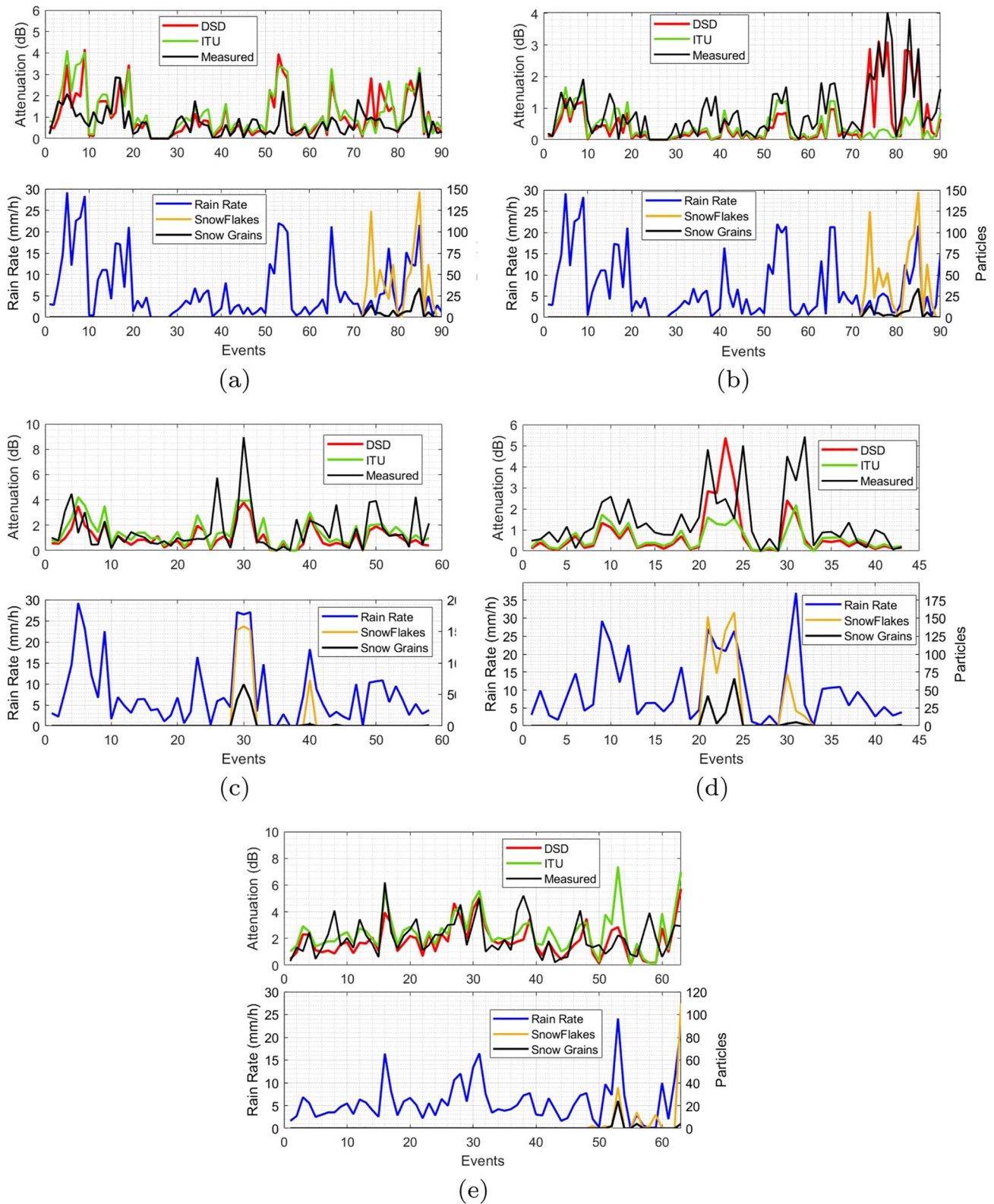


Figure 12. Samples of measured rain attenuation compared to drop size distribution and International Telecommunication Union models over predominant rainfall events for K and E band at direct and side 36 m link and for E band at Filtronic 200 link: (a) E band 36 m direct link, (b) K band 36 m direct link, (c) E band 36 m side link, (d) K band 36 m side link, and (e) E band 200 m link.

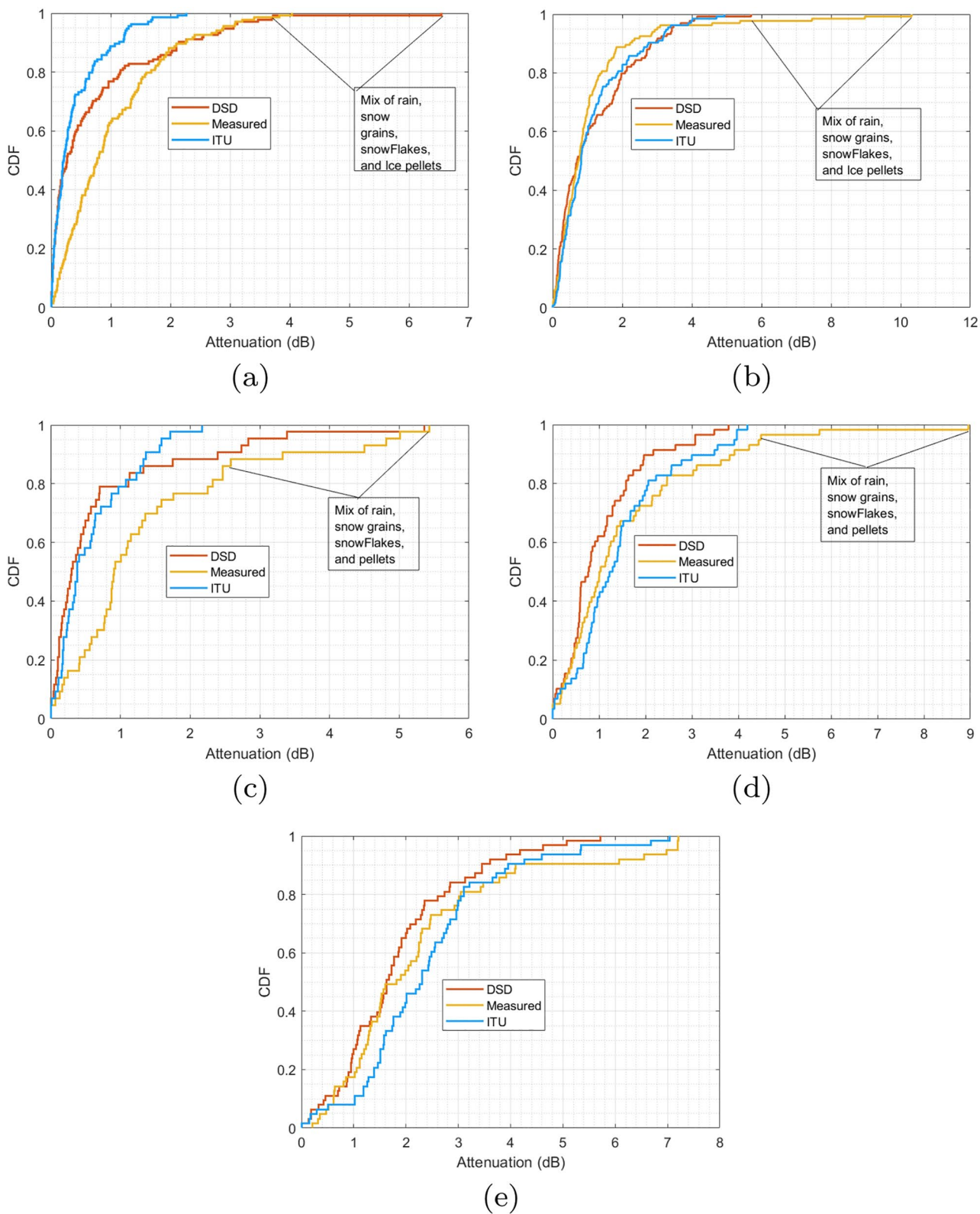
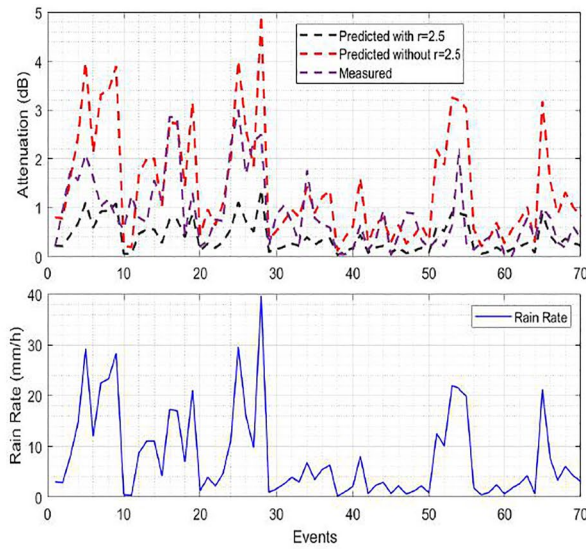
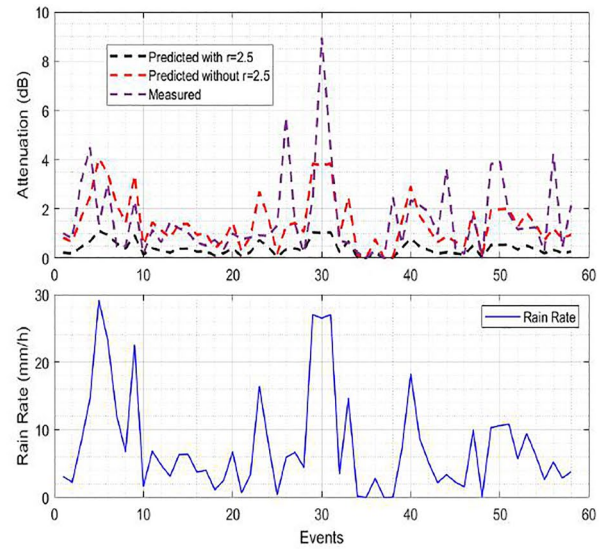


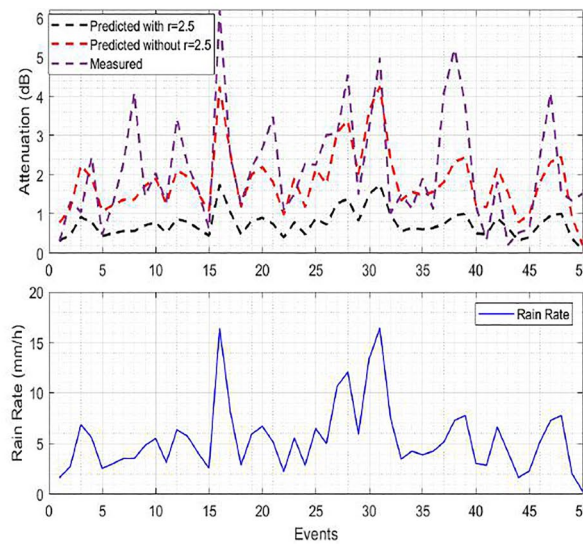
Figure 13. CDFs of the measured and the predicted rain attenuation for the three links: (a) K band 36 m direct link, (b) E band 36 m direct link, (c) K band 36 m side link, (d) E band 36 m side link, and (e) E band 200 m Filtronic link.



(a) E band 36 m direct link.



(b) E band 36 m side link.

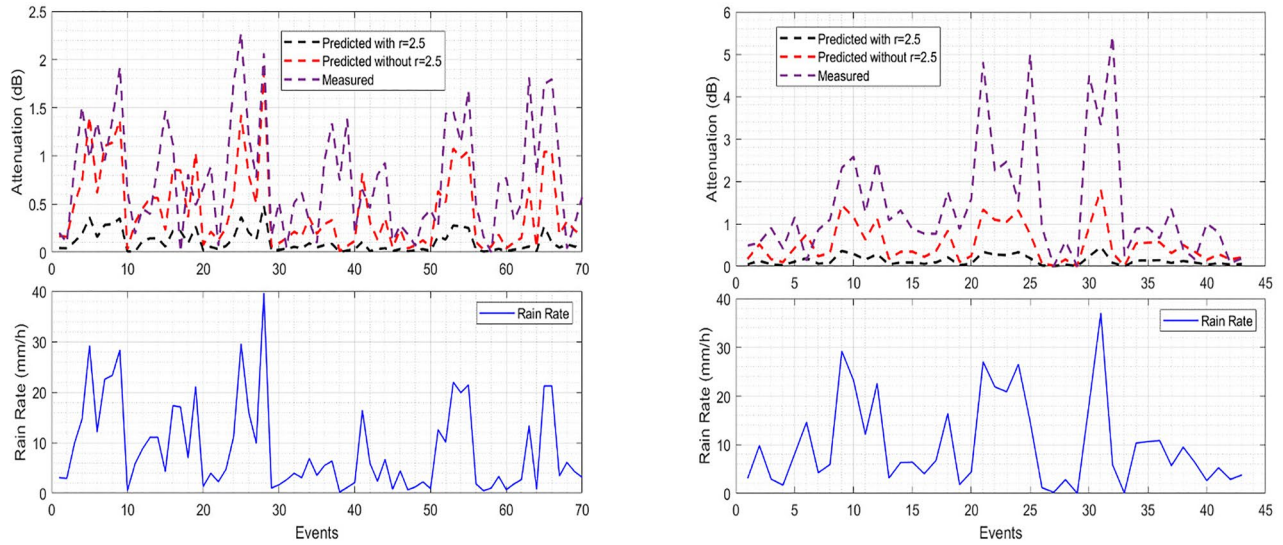


(c) E band 200 m link.

Figure 14. Measured and International Telecommunication Union predicted rain attenuation for E band for the three links with and without using the maximum distance factor restriction r of 2.5: (a) E band 36 m direct link, (b) E band 36 m side link, and (c) E band 200 m link.

depends on frequency and temperature. These parameters identify the scattering modeling which can be divided into single-scattering or multiple-scattering. Single scattering considers one interaction between the incident wave and the precipitation field. When the density of scatterers or the scattering cross section increases multiple scattering occurs. In the current analysis, the most common first order rain scattering approach is adopted. The regular model which is considered widely to cause interference between fixed links (Capsoni et al., 2010) is presented in Figure 17.

Spherical raindrops, Mie theory, and bistatic radar equation given in Capsoni et al. (2010) and Capsoni and D'Amico (1991) are considered for scattering functions calculations. The following functions are derived from Mie theory and describe wave scattering through a common raindrops geometry:



(a) K band 36 m direct link.

(b) K band 36 m side link.

Figure 15. Measured and International Telecommunication Union predicted rain attenuation for K band for the two links with and without using the maximum distance factor restriction r of 2.5: (a) K band 36 m direct link and (b) K band 36 m side link.

1. Mie scattering amplitude function is given by:

$$S_1(\cos\theta) = \sum_{n=1}^{\infty} \frac{2n+1}{n(n+1)} (a_n \pi_n + b_n \tau_n) \quad (10)$$

$$S_2(\cos\theta) = \sum_{n=1}^{\infty} \frac{2n+1}{n(n+1)} (a_n \tau_n + b_n \pi_n) \quad (11)$$

the functions $\pi_n(\cos\theta)$ and $\tau_n(\cos\theta)$ describe the angular scattering patterns. a_n and b_n are Mie coefficients complex functions of drop diameter, refractive index, and wavelength.

2. Scattering cross section. It gives a conjectural definition of how much area is blocked out by the target during the raindrops scattering event. It is given by:

$$\sigma_{sca} = \frac{\pi D^2}{x^2} \sum_{n=1}^{\infty} (2n+1) (|a_n|^2 + |b_n|^2) \quad (12)$$

Figure 18 shows the calculated scattering cross section as a function of scattering angle. The scattering cross section reaches a value of 1.04×10^{-4} (m^2/m^3) for a scattering angle of 0° at very heavy rainfall. Operating at higher rain intensity will introduce superior scattering for both bands.

3. Bistatic scattering cross section η per unit volume which is a function of frequency and scattering geometry of raindrops

$$\eta(\theta_s) = \int_0^{\infty} N(D) \sigma_{sca}(D) P(D, \theta_s) dD \quad (13)$$

θ_s is the scattering angle, $N(D)$ is the measured raindrops distribution. One significant element that defines the prospect distribution of the scattered wave direction is the scattering phase function $P(D, \theta_s)$ defined by:

$$P(\theta) = \frac{|S_1(\theta)|^2 + |S_2(\theta)|^2}{\pi x^2 Q_{sca}} \quad (14)$$

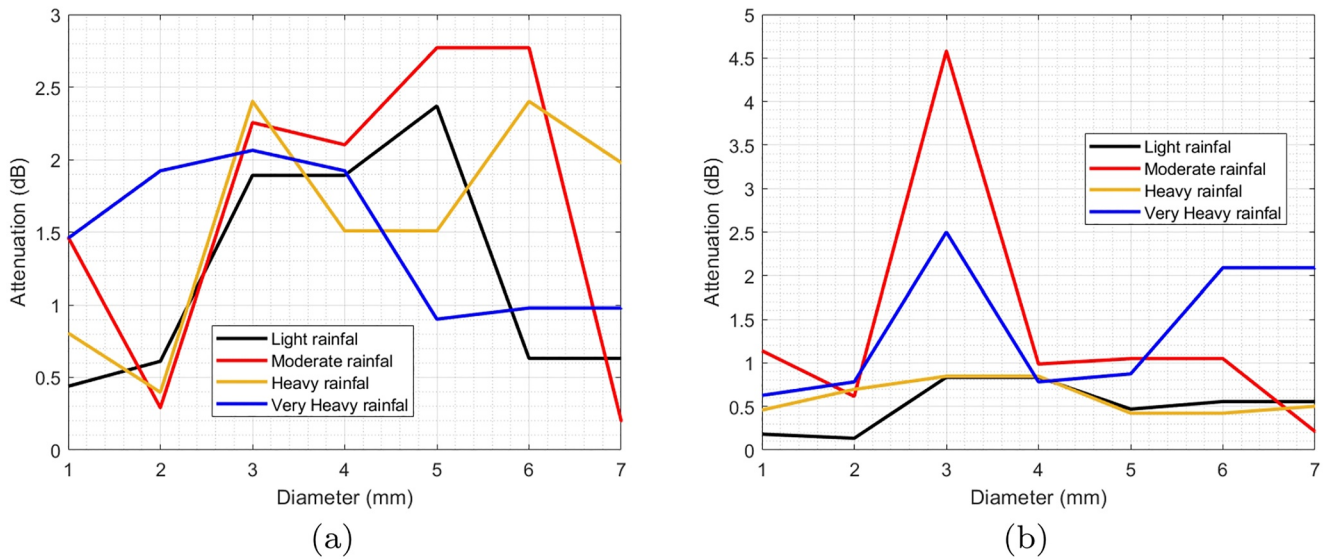


Figure 16. Calculated attenuation versus raindrop diameter in mm for (a) 25.84 GHz and (b) 77.54 GHz.

where $S1(\theta)$ and $S2(\theta)$ terms are elements of the scattering amplitude matrix given by the Mie theory. Figure 19 shows the scattering phase function versus the scattering angle for predefined raindrops diameter dominant in the disdrometer measurements. It is noticed from the figure that the 77 GHz band is considerably forward oriented pattern while at 26 GHz it is more inclined to Rayleigh, which explains the difference between the measured and predicted attenuation for the K band side link presented in the previous section when Mie theory was applied for all the calculations of both bands.

Figure 20 displays the behavior of the bistatic scattering cross section for the E band versus the scattering angle for the two different rainfall rates: 16 and 39 mm/hr. The rain-induced scattering is due to the beam angle falling below 60° . It is the region where it is having significant effect but confined only to rainfall events higher than 10 mm/hr and considerable raindrops diameter above 1 mm.

6. Conclusions

Rain attenuation for millimeter wave 5G fixed link applications was investigated using long-term rain statistics and radio data collected over three fixed links at Durham University. For most rain events, the signal level tends to follow the trend of rainfall, and rain attenuation rises as the rain intensity increases. Predicted attenuation values from the DSD and the ITU models have been analyzed and compared to measured data at 22.84 and 77.54 GHz for a direct and a side link over 36 m together with a 200 m point to point link at 77.125 GHz. The DSD proves

that rainfall rates are insufficient to estimate rain attenuation values as other factors are involved such as the raindrops shape and distribution, number of dominant drops, diameter, and velocity. The drops diameter in the range of 0.1–2 mm contributes to the overall attenuation within all frequencies for particle speeds in the range between 1 and 5 m/s. Larger raindrops contribute irregularly to the attenuation when the rainfall velocity and particle speed is in the range of (5–10 m/s). Measurement results using the long-term measurements over the short-range fixed links indicate that using recommendation ITU-R P.530-18 without the restricted distance factor recommended in P.530-17 gives attenuation values closer to the measured values. In future work, further measurements will be analyzed to better investigate the path reduction factor value with specific consideration of the spatial homogeneity of precipitation along the path and of any additional effects inducing supplementary attenuation on the link such as wet antenna and/or due to the system, which, as the path length decreases, are expected to be critical for

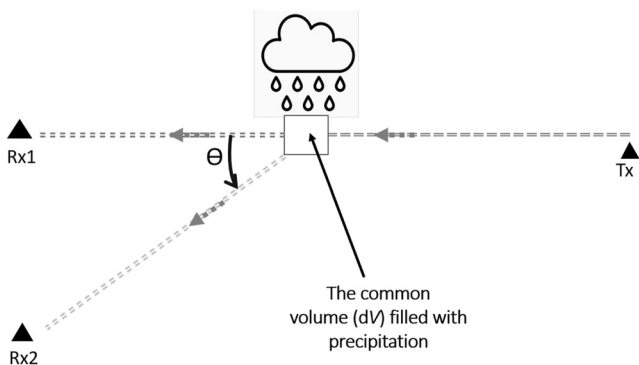


Figure 17. Geometry of rain scatter.

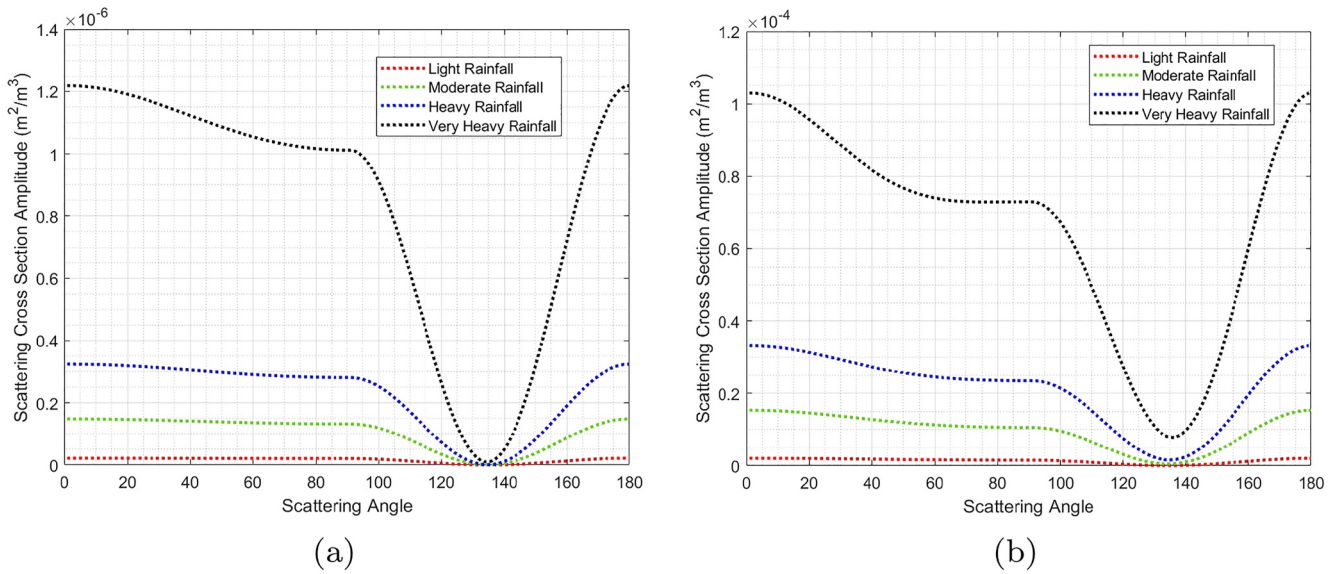


Figure 18. The scattering cross section calculated as a function of the scattering angle: (a) 25.84 GHz and (b) 77.54 GHz.

the isolation of the impact solely due to rain. In this paper a simplified approach of raindrops induced scattering was introduced to minimize the calculation complexity. Data indicate that the scattering cross section varies over a wide range between 0° and 180° and symmetrically to 360° . Further work is ongoing to study the interference between cross-polarization links, along with an evaluation of other precipitation effects such as snow grains, snowflakes, hail, ice pellets, graupel, wind, and humidity on rain attenuation and scattering.

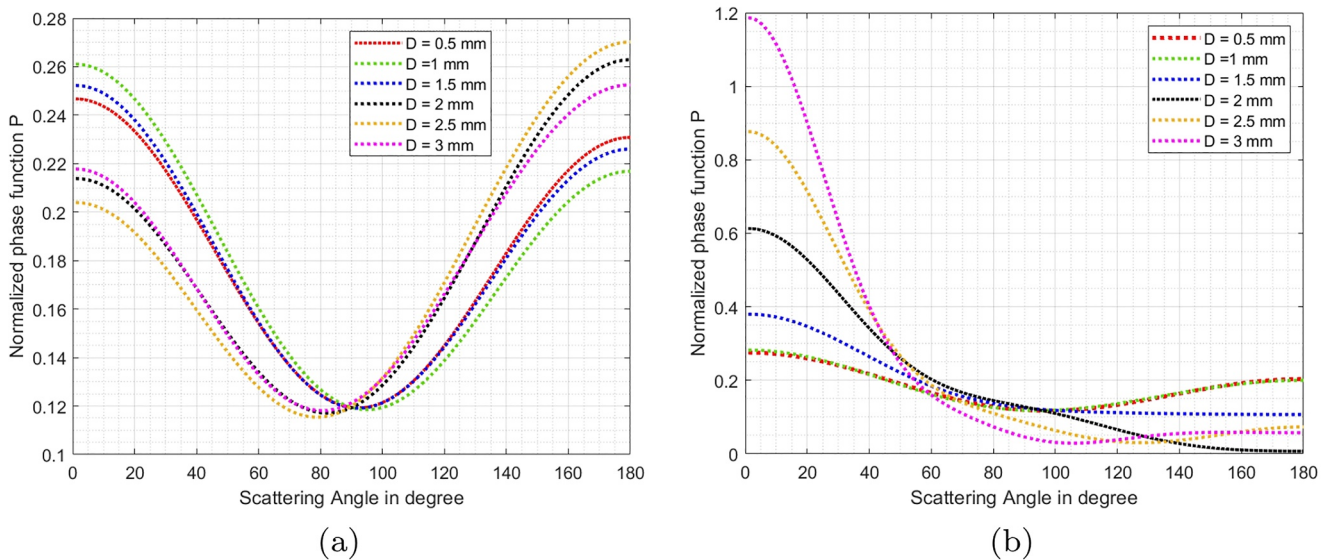


Figure 19. Normalized scattering phase function $P(\theta)$ at: (a) 25.84 GHz and (b) 77.54 GHz.

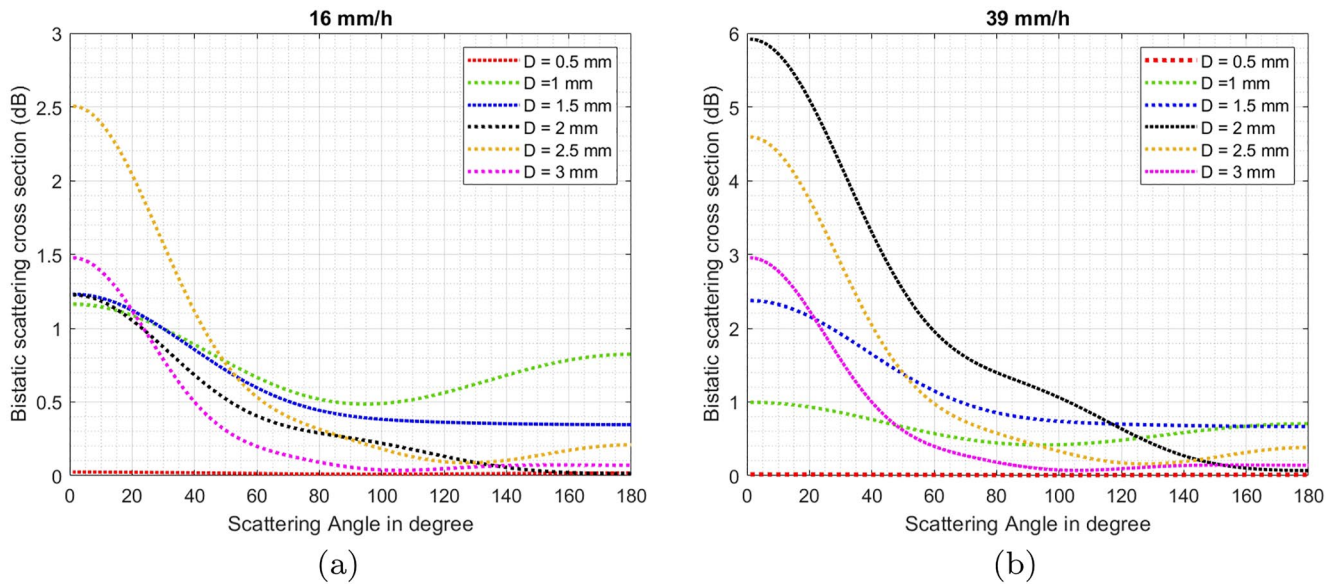


Figure 20. Example of E band bistatic scattering cross section at two different rainfall: (a) 16 mm/hr and (b) 39 mm/hr.

Data Availability Statement

The data that support the findings of this study will be submitted to the ITU-R Study Group 3 data bank (DBSG-3) and availability is subject to ITU-R policy: <https://www.itu.int/en/ITU-R/study-groups/rsg3/Pages/dtbank-dbsg3.aspx>.

Acknowledgments

The authors would like to acknowledge the support of WaveComBE project, under Horizon 2020 research and innovation program with grant agreement No. 766231, the support from Ofcom under grant No. 1362, and the technicians at Durham University for the setup of the weather station and fixed links. The 200 m radio link was set up with the support of Filtronic who provided the RF heads. The authors would also like to acknowledge Mohamed Abdulali at Durham University for developing C code for automatic data acquisition.

References

- Åsen, W., & Gibbins, C. J. (2002). A comparison of rain attenuation and drop size distributions measured in Chilbolton and Singapore. *Radio Science*, 37(3), 6-1-6-15. <https://doi.org/10.1029/2000RS002613>
- Atlas, D., Srivastava, R. C., & Sekhon, R. S. (1973). Doppler radar characteristics of precipitation at vertical incidence. *Reviews of Geophysics and Space Physics*, 11(1), 1-35. <https://doi.org/10.1029/RG011i001p00001>
- Atlas, D., & Ulbrich, C. W. (1977). Path- and area-integrated rainfall measurement by microwave attenuation in the 1-3 cm band. *Journal of Applied Meteorology*, 16(20), 1322-1331. [https://doi.org/10.1175/1520-0450\(1977\)016<1322:PAAIRM>2.0.CO;2](https://doi.org/10.1175/1520-0450(1977)016<1322:PAAIRM>2.0.CO;2)
- Aydin, K., & Daisley, S. E. A. (2002). Relationships between rainfall rate and 35-GHz attenuation and differential attenuation: Modeling the effects of raindrop size distribution, canting, and oscillation. *IEEE Transactions on Geoscience and Remote Sensing*, 40(11), 2343-2352. <https://doi.org/10.1109/TGRS.2002.805073>
- Bohren, C., & Huffman, D. R. (1998). *Absorption and scattering of light by small particles*. Wiley Science Paperback Series.
- Brazda, V., & Fiser, O. (2015). Comparison of exact and approximate FSO rain attenuation formulas based on actual DSD. In *2015 9th European Conference on Antennas and Propagation (EUCAP)* (pp. 1-5). IEEE.
- Budalal, A. A. H., Islam, M. R., Abdullah, K., & Abdul Rahman, T. (2020). Modification of distance factor in rain attenuation prediction for short-range millimeter-wave links. *IEEE Antennas and Wireless Propagation Letters*, 19(6), 1027-1031. <https://doi.org/10.1109/LAWP.2020.2987462>
- Capsoni, C., & D'Amico, M. (1991). Prediction of effective transmission loss by hydrometeor scatter through a 3D rain cell model. In *1991 7th International Conference on Antennas and Propagation, ICAP 91 (IEE)* (Vol. 1, pp. 238-241).
- Capsoni, C., Luini, L., & D'Amico, M. (2010). The MultiEXCELL model for the prediction of the radio interference due to hydrometeor scattering. In *Proceedings of the 4th European Conference on Antennas and Propagation* (pp. 1-5). IEEE.
- Carlton, W. U. (1983). Natural variations in the analytical form of the raindrop size distribution. *Journal of Climate and Applied Meteorology*, 22(10), 1764-1775. [https://doi.org/10.1175/1520-0450\(1983\)022<1764:NVITAF>2.0.CO;2](https://doi.org/10.1175/1520-0450(1983)022<1764:NVITAF>2.0.CO;2)
- Chandra Kestwal, M., Joshi, S., & Singh Garia, L. (2014). Prediction of rain attenuation and impact of rain in wave propagation at microwave frequency for tropical region (Uttarakhand, India). *International Journal of Microwave Science and Technology*, 2014, 1-6. <https://doi.org/10.1155/2014/958498>
- Crane, R. K. (2003). *Propagation handbook for wireless communication system design* (1st ed.). CRC Press.
- Durgin, G. D. (2000). *Theory of stochastic local area channel modeling for wireless communications* (Doctoral dissertation). Retrieved from <http://hdl.handle.net/10919/29843>
- Han, C., & Duan, S. (2019). Impact of atmospheric parameters on the propagated signal power of millimeter-wave bands based on real measurement data. *IEEE Access*, 7, 113626-113641. <https://doi.org/10.1109/ACCESS.2019.2933025>
- Hemadneh, I. A., Satyanarayana, K., El-Hajjar, M., & Hanzo, L. (2017). Millimeter-wave communications: Physical channel models, design considerations, antenna constructions, and link-budget. *IEEE Communications Surveys & Tutorials*, 20(2), 870-913. <https://doi.org/10.1109/COMST.2017.2783541>

- Huang, J., Cao, Y., Raimundo, X., Cheema, A., & Salous, S. (2019). Rain statistics investigation and rain attenuation modeling for millimeter wave short-range fixed links. *IEEE Access*, 7, 156110–156120. <https://doi.org/10.1109/access.2019.2949437>
- ITU-WRC. (2019). *Final acts of the World Radiocommunication Conference (WRC-19) (recommendation)*. International Telecommunication Union (ITU).
- Jürg, J., & Enrico, G. G. (1978). Shapes of raindrop size distributions. *Journal of Applied Meteorology*, 17(7), 1054–1061. [https://doi.org/10.1175/1520-0450\(1978\)017<1054:sorsd>2.0.co;2](https://doi.org/10.1175/1520-0450(1978)017<1054:sorsd>2.0.co;2)
- Juttula, H., Kokkonen, J., Lehtomaki, J., Makynen, A., & Juntti, M. (2019). Rain induced co-channel interference at 60 GHz and 300 GHz frequencies. In *2019 IEEE International Conference on Communications workshops (ICC workshops)* (pp. 1–5). <https://doi.org/10.1109/ICCW.2019.8756966>
- Kim, J. H., Jung, M.-W., Yoon, Y. K., & Chong, Y. J. (2013). The measurements of rain attenuation for terrestrial link at millimeter wave. In *2013 International Conference on ICT Convergence (ICTC)* (pp. 848–849). <https://doi.org/10.1109/ICTC.2013.6675497>
- Kumar, L. S., Lee, Y. H., & Ong, J. T. (2010). Truncated gamma drop size distribution models for rain attenuation in Singapore. *IEEE Transactions on Antennas and Propagation*, 58(4), 1325–1335. <https://doi.org/10.1109/TAP.2010.2042027>
- Kvicera, V., Grabner, M., & Fiser, O. (2011). 4-year hydrometeor attenuation statistics obtained at 93 GHz on an 850 m terrestrial path. In *Proceedings of the 5th European Conference on Antennas and Propagation (EUCAP)* (pp. 2501–2503). IEEE.
- Lam, H. Y., Luini, L., Din, J., Alhilali, M. J., Jong, S. L., & Cuervo, F. (2017). Impact of rain attenuation on 5G millimeter wave communication systems in equatorial Malaysia investigated through disdrometer data. In *2017 11th European Conference on Antennas and Propagation (EUCAP)* (pp. 1793–1797). <https://doi.org/10.23919/EuCAP.2017.7928616>
- Luini, L., Roveda, G., Zaffaroni, M., Costa, M., & Riva, C. (2018). EM wave propagation experiment at E band and D band for 5G wireless systems: Preliminary results. In *12th European Conference on Antennas and Propagation (EUCAP 2018)* (pp. 1–5). <https://doi.org/10.1049/cp.2018.0378>
- Marshall, J. S., & Palmer, W. M. (1948). The distribution of raindrops with size. *Journal of the Atmospheric Sciences*, 5(4), 165–166. [https://doi.org/10.1175/1520-0469\(1948\)005<0165:TDORWS>2.0.CO;2](https://doi.org/10.1175/1520-0469(1948)005<0165:TDORWS>2.0.CO;2)
- Mora Navarro, K. M., & Costa, E. (2016). Interference between millimeter wave radio links due to rain scatter. In *2016 USNC-URSI Radio Science Meeting* (pp. 115–116). <https://doi.org/10.1109/USNC-URSI.2016.7588539>
- Nabangala, M. (2016). *Determination of rainfall parameters for specific attenuation due to rain for different integration times for terrestrial line-of-sight links in South Africa* (PhD thesis). University of KwaZulu-Natal.
- Nazar Elfadil, M., Zia, N., Salam, M. A., & Rao, J. (2005). Microwave attenuation studies due to rain for communication links operating in Malaysia. *Georgian Electronic Scientific Journal: Computer Science and Telecommunications*, 5(1), 9–17.
- Olsen, R. L., Rogers, D. V., & Hodge, D. B. (1978). The aR^b relation in the calculation of rain attenuation. *IEEE Transactions on Antennas and Propagation*, 26(2), 318–329. <https://doi.org/10.1109/TAP.1978.1141845>
- Olsen, R. L., Rogers, D. V., Hulays, R. A., & Kharadly, M. M. Z. (1993). Interference due to hydrometeor scatter on satellite communication links. *Proceedings of the IEEE*, 81(6), 914–9229. <https://doi.org/10.1109/5.257688>
- Recommendation ITU-R P.838-3. (2005). *Specific attenuation model for rain for use in prediction methods* (Technical Report). ITU.
- Salous, S., Cao, Y., & Raimundo, X. (2019). Impact of precipitation on millimeter wave fixed links. In *2019 13th European Conference on Antennas and Propagation (EUCAP)* (pp. 1–4). IEEE.
- Sander, J. (1975). Rain attenuation of millimeter waves at $\lambda = 5.77, 3.3,$ and 2 mm. *IEEE Transactions on Antennas and Propagation*, 23(2), 213–220. <https://doi.org/10.1109/TAP.1975.1141059>
- Saurabh, D., Animesh, M., & Ashish, S. (2010). Rain attenuation modeling in the 10–100 GHz frequency using drop size distributions for different climatic zones in tropical India. *Progress in Electromagnetics Research B*, 25(25), 211–224. <https://doi.org/10.2528/PIERB10072707>
- Schiebener, P., Straub, E. J., Levelt Sengers, J. M. H., & Gallagher, J. S. (1990). Refractive index of water and steam as function of wavelength, temperature and density. *Journal of Physical and Chemical Reference Data*, 19(3), 677–717. <https://doi.org/10.1063/1.555859>
- Schleiss, M., Rieckermann, J., & Berne, A. (2013). Quantification and modeling of wet-antenna attenuation for commercial microwave links. *IEEE Transactions on Geoscience and Remote Sensing*, 10(5), 1195–1199. <https://doi.org/10.1109/lgrs.2012.2236074>
- Schönhuber, M., Plimon, K., & Thurai, M. (2015). Statistical significance of specific rain attenuation dependence on geographic and climatic conditions. In *2015 9th European Conference on Antennas and Propagation (EUCAP)* (pp. 1–5). IEEE.
- Scientific, C. (2015). Pws100 present weather sensor [Computer software manual]. Campbell Scientific.
- Setijadi, E., Matsushima, A., Tanaka, N., Hendrantoro, G., & Elektro, J. T. (2009). Effect of temperature and multiple scattering on rain attenuation of electromagnetic waves by a simple spherical model. *Progress in Electromagnetics Research*, 339–354, 339–354. <https://doi.org/10.2528/PIER09102609>
- Shrestha, S., & Choi, D.-Y. (2017). Rain attenuation statistics over millimeter wave bands in South Korea. *Journal of Atmospheric and Solar-Terrestrial Physics*, 152, 1–10. <https://doi.org/10.1016/j.jastp.2016.11.004>
- Surco Espejo, T. M., & Costa, E. (2017). Scattering due to rain in Brazil for millimeter waves. In *2017 SBMO/IEEE MTT-S International Microwave and Optoelectronics Conference (IMOC)* (pp. 1–5). <https://doi.org/10.1109/IMOC.2017.8121140>
- Tamošinitait, M., Tamošinas, S., & Žilinskas, M. (2011). Atmospheric attenuation due to humidity. In P. V.Zhurbenko (Ed.), *Electromagnetic waves* (pp. 158–169). In Tech.
- Townsend, A. J., Watson, R. J., & Hodges, D. D. (2009). Analysis of the variability in the raindrop size distribution and its effect on attenuation at 20–40 GHz. *IEEE Antennas and Wireless Propagation Letters*, 8(2), 1210–1213. <https://doi.org/10.1109/LAWP.2009.2035724>
- Tuhina, H., Adhikari, A., & Maitra, A. (2018). Rain attenuation studies from radiometric and rain DSD measurements at two tropical locations. *Journal of Atmospheric and Solar-Terrestrial Physics*, 170, 11–20. <https://doi.org/10.1016/j.jastp.2018.02.004>
- Zahid, O., Huang, J., & Salous, S. (2020). Long term rain attenuation measurements at millimeter wave bands for direct and side short-range fixed links. In *2020 33rd General Assembly and Scientific Symposium of the International Union of Radio Science* (pp. 1–4). <https://doi.org/10.23919/URSIGASS49373.2020.9232024>